Chemistry–A European Journal
Research Article
doi.org/10.1002/chem.202403695
Chemistry Europe
European Chemical Societies Publishing
www.chemeurj.org

Unraveling Mechanism and Enhancing Selectivity of a Ru^{II}-bis-bipyridyl-morphocumin Complex with RAFT-Generated Glycopolymer Exploiting Warburg Effect in Cancer

Souryadip Roy,[a] Soumya Paul,[a] Sujato Mukherjee,[a] Priyadarsi De,[a] and Arindam Mukherjee*[a]

The Warburg effect, which generates increased demand of glucose in cancer cells is a relatively underexplored phenomenon in existing commercial drugs to enhance uptake in cancer cells. Here, we present a chemotherapeutic strategy employing a Ru(II)-bis-bipyridyl-morphocumin complex (**2**) encapsulated in a self-assembling glucose-functionalized copolymer P(G-EMA-*co*-MMA) (where G = glucose; MMA = methyl methacrylate; EMA = ethyl methacrylate), designed to exploit this effect for enhanced selectivity in cancer treatment. The P(G-EMA-*co*-MMA) polymer, synthesized *via* reversible-addition fragmentation chain transfer (RAFT) polymerization, has a number average molecular weight ($M_{n,NMR}$) of 8000 g/mol. Complex **2**, stable in aqueous media, selectively releases a cytotoxic, lysosome-targeting compound, morphocumin, in the presence of excess hydrogen peroxide (H_2O_2), a reactive oxygen species (ROS) prevalent in tumor microenvironments. Additionally, complex **2** promotes ROS accumulation, which may further enhance morphocumin release through a synergistic domino effect. Comparative studies reveal that **2** outperforms its curcumin Ru(II) complex (**1**) analog in solution stability, organelle specificity, and cellular mechanisms. Both **1** and **2** exhibit phototherapeutic effects under low-intensity visible light, but their chemotoxicity significantly increases with incubation time in the dark, highlighting the superior chemotherapeutic efficacy of the *O,O*-coordinating Ru(II) ternary polypyridyl complexes. Complex **2** induces apoptosis *via* the intrinsic pathway and shows a 9-fold increase in selectivity for pancreatic cancer cells (MIA PaCa-2) over non-cancerous HEK293 cells when encapsulated in the glucose-conjugated polymer (**DP@2**). Glucose deprivation in the culture medium further enhances drug efficacy by an additional 5-fold. This work underscores the potential of glucose-functionalized polymers and ROS-responsive Ru(II) complexes in targeted cancer therapy.

Introduction

Over decades, researchers have delved into the complexities of cancer, progressively gaining deeper insights. Among the array of drugs utilized in cancer chemotherapy, platinum complexes have exhibited significant success with dominance, albeit accompanied by severe side effects, a common drawback shared among most anti-cancer medications.[1] Notably, the soft nature of Pt(II) is exploited by cancer cells, rendering the drugs less effective by coordinating with thiols from various small molecules and proteins abundant in cancer cells (e.g., glutathione, ATP7B, MMP, thioredoxin, etc.). In the quest for non-Pt(II) anti-cancer agents, Ru(II) presents a promising alternative due to its lower softness stemming from a greater charge/radius ratio rendering subtle preferential differences in coordination environment, which impart suitable biological properties, thereby advocating its potential candidacy in cancer therapeutics.[2,3] To exploit kinetic inertness and mitigate dosage loss due to thiol-based sequestration, researchers are drawn to the potential of Ru polypyridyl complexes. These complexes offer straightforward synthesis, exceptional stability, a broad range of photophysical and photochemical properties, and significant activity in biological systems.[4,5] $[Ru(bpy)_3]Cl_2$ was the first reported ruthenium polypyridyl complex by Burstall in 1936[6] but gained prominence in the early 1980s for capability of water splitting through the 'ruthenium blue dimer' $[(bpy)_2Ru(H_2O)(\mu\text{-}O)(H_2O)Ru(bpy)_2]^{4+}$.[7] In the past decade, Ru polypyridyl complexes have emerged as promising metal-based anticancer agents, particularly in photodynamic therapy (PDT).[8–10] This interest was further fueled by the entry of the first Ru(II)-based polypyridine, TLD-1433, into phase II clinical trials for non-muscle invasive bladder cancer.[10,11] Various research groups have highlighted the potential of these complexes in both PDT and photoactivated chemotherapy (PACT).[12,13] PACT, also known as 'photocaged complexes', involves molecular changes upon photoirradiation, offering several advantages over traditional PDT. Ru polypyridyl complexes with bioactive ligands are particularly advantageous for PACT, as both the aquated Ru polypyridyl and the photo-dissociated ligand can synergistically target the tumor microenvironment upon photoirradiation.[14,15]

Natural products used in food are in general well tolerant to humans and have consistently held a role in drug design as bioactive ligands. Curcumin, one of the most investigated natural products is a food additive that may be taken up to

[a] S. Roy, S. Paul, S. Mukherjee, P. De, A. Mukherjee
Centre for Advanced Functional Materials, Department of Chemical Sciences, Indian Institute of Science Education and Research Kolkata, Nadia, West Bengal, Mohanpur 741246, India
E-mail: a.mukherjee@iiserkol.ac.in

Supporting information for this article is available on the WWW under https://doi.org/10.1002/chem.202403695

3 mg/kg body weight per day.[16] The dose tolerance limit of curcumin and its derivatives is influenced by the toxic products formed due to its physiological instability.[17,18] Numerous studies have documented the targeted discharge of curcumin within cancer cells, yet the challenge persists due to curcumin's instability in physiological environments. Consequently, to achieve selective release of a curcumin derivative, it is imperative for it to remain stable within the tumor microenvironment. Morphocumin is designed to be physiologically stable, better soluble, lysosome targeting photoactive curcumin analogue with pronounced phototherapeutic properties.[19] Hence, we chose Morphocumin as the bioactive ligand for this work.

Apart from external photo stimuli, several other factors are the foundation of ligand ejection that generally differentiates cancer cells from normal cells i.e., pH variation, reactive oxygen species (ROS) overexpression, redox activity and enzyme overexpression.[20] An elevated amount of ROS in hypoxic tumors is a defense mechanism for survival and can be modulated as a therapeutic advantage. The most frequently elevated ROS include hydroperoxide ($H\dot{O}^{-}$), superoxide ($O_2^{\bullet -}$), and hydroxyl radical ($\dot{O}H$).[21] Apart from the above, hydrogen peroxide (H_2O_2), is a potent compound capable of generating ROS, with chemical stability needed to set up notable steady-state concentrations *in vivo*. Large amounts of H_2O_2 are reportedly produced *in vitro* without exogenous stimulation in several human carcinoma cell lines, including malignant melanoma, colon carcinoma, pancreatic carcinoma, neuroblastoma, breast carcinoma, and ovarian carcinoma.[22,23] H_2O_2 freely passes through membranes and can reach any cellular compartment.[24] Apparently human tumor cell lines constitutively generate H_2O_2 at rates (up to 0.5 nmol/10^4 cells/h) that cumulatively amount at 4 h to the amount of H_2O_2 produced by phorbol ester-triggered neutrophils.[22] This excess availability of H_2O_2 in cancer cells over normal cells allows the exploitation of H_2O_2 as a potential therapeutic target. Thus, in recent years, there have been reports of utilizing H_2O_2 stimulation to release a drug attached to a prodrug.[25,26]

Small molecule metal complexes may often encounter challenges associated with poor solubility and stability in the biological milieu, and exhibit undesired side effects resulting from non-specific uptake in the body.[27] Consequently, their therapeutic efficacy is often compromised. To address the challenges of solubility, stability, and cellular uptake associated with small molecule complexes, especially Ru(II) in particular, researchers are developing advanced drug delivery systems aimed to improve the activity and selectivity of the compounds.[28–30] In contrast to traditional systemic treatment approaches that rely on using small molecule as drugs, encapsulating them within nanoscale delivery vehicle can significantly enhance their stability and reduce systemic toxicity. This is achieved by preventing early degradation and non-specific interactions with healthy tissues, enhancing drug solubility, and allowing for longer circulation times in the bloodstream.[31] Therefore, encapsulating drugs within natural or synthetic polymeric nanoparticles that impart stability and selectivity are emerging as a promising strategy.[29,32–34] This approach enhances the therapeutic efficacy of the potential chemotherapeutic agents by improving their solubility, biocompatibility, biodistribution, and circulation time within the body.[35] Additionally, the polymeric nanocarriers serve to reduce the biodegradation of the drugs before reaching the targeted site of action.

Typically, cancer cells exhibit higher glucose uptake and metabolism because of their rapid growth and metastatic nature. Therefore, various human cancer cells including breast, pancreatic, ovarian, lung, and cervical cancer cells possess overexpression of glucose transporters (GLUTs).[36] Thus, targeting GLUTs using glucose-based polymeric nanoparticles, suitable for encapsulating drugs, to facilitate endocytosis within cancer cells is a suitable approach for drug delivery in cancer therapy.[31] Glycopolymers consist of a synthetic polymer backbone adorned with sugar moieties, and they have garnered significant attention because of the high specificity of carbohydrates for sugar-binding proteins that are overexpressed on cancer cell surfaces. This characteristic enables the targeting and delivery of drugs to cancer cells through receptor-mediated endocytosis.[37,38]

Herein, we report Ru bis-bipyridyl complexes of curcumin and morphocumin differentiating their chemotherapeutic vs. photodynamic behavior, dependence of the activity on the *O*,*O*-coordinating curcumin derivatives coordinating to the Ru bis-bipyridyl precursor. Among the two complexes of the formulation $[Ru(bpy)_2(curcumin)]PF_6$ (**1**) and $[Ru(bpy)_2(morphocumin)]PF_6$ (**2**), complex **2** display better aqueous-stability and releases the stable lysosome targeting morphocumin in the presence of excess H_2O_2, a viable therapeutic target to enhance cytotoxicity towards ROS rich cancer cells. The altered metabolism of neoplastic cells with accelerated glycolysis, termed as 'Warburg effect'[39] leading to overexpression of GLUTs was further exploited by delivering **2** using glucose functionalized polymeric nanoparticles (GFPNs)[40,41] showcasing enhanced selectivity towards cancer cells (Figure 1).

Results and Discussion

Synthesis and Characterization of 1 and 2

To capitalize the precedence of Ru polypyridyl complexes over arene analogs, viz. strong visible light absorption, greater ROS generation efficiency, enhanced photophysical properties, stability and biocompatibility we designed simple Ru(II) bis-bipyridyl complexes of *O*,*O*-coordinating ligands.[42] Two Ru complexes (**1** and **2**) were synthesized in good yields (78% and 69% respectively) by reacting the corresponding *O*,*O*-coordinating ligands curcumin and morphocumin with equimolar $Ru(bpy)_2Cl_2$ and 1.5 equivalent triethylamine in a 1:1 ethanol-water mixture following reported protocol[43] as depicted in Scheme 1. COMMENT: This scheme 1 needs to be replaced with uploaded Scheme 1 as charges on PF6 were in wrong position and one Cl coordinated to Ru(II) became HCl which is rectified in the uploaded scheme 1 Complex **1** was previously reported

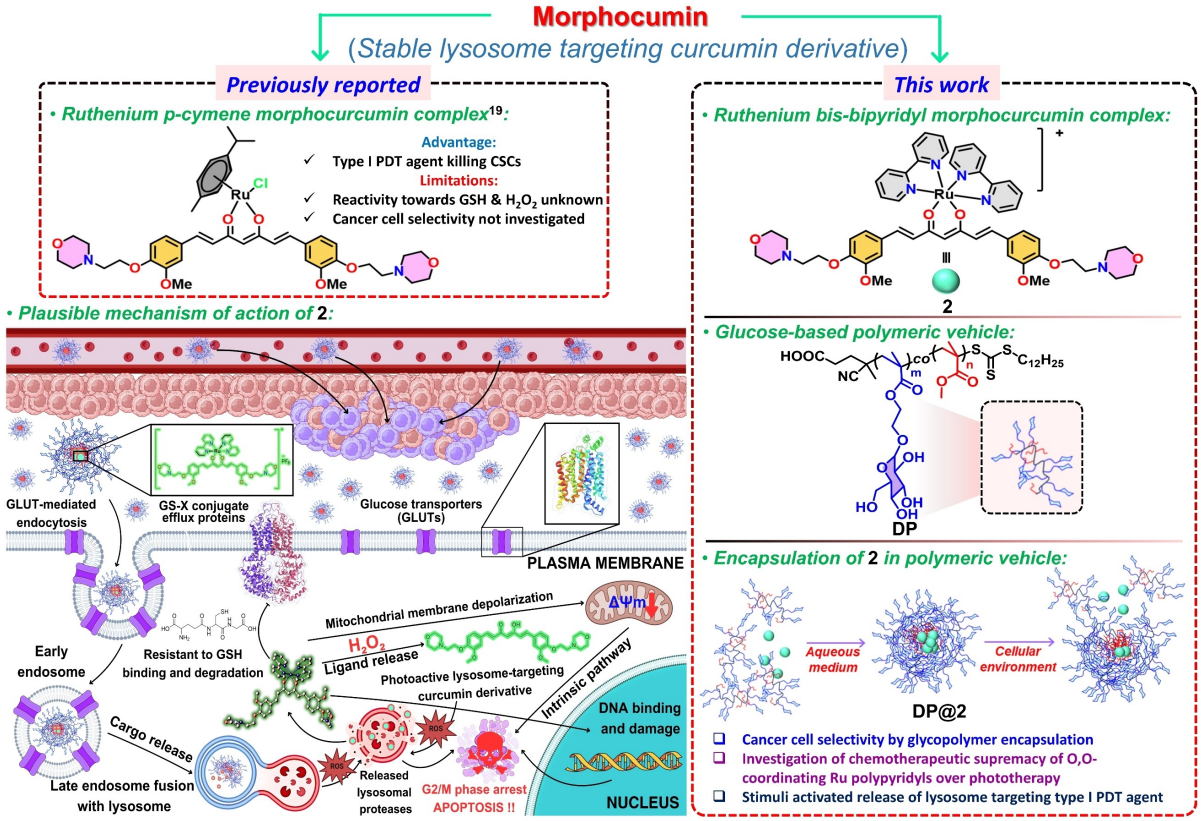

Figure 1. Chemical structures of the previously studied Ru(II) *p*-cymene-morphocumin complex (**2**) and the Ru(II) bis-bipyridyl complexes of morphocumin presented in this work along with a schematic representation of the **2** encapsulated glucose functionalized polymers generating nanoparticle formulations and a probable mechanistic representation of the cellular mechanism of action.

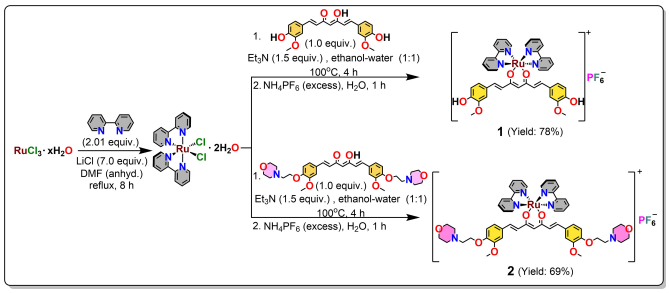

Scheme 1. Schematic representation of the synthesis of **1** and **2** from curcumin and morphocumin.

and we used it as a standard.[44] These complexes were characterized by standard analytical techniques including NMR, ESI-HRMS, FT-IR, UV-Vis, and fluorescence spectroscopy (Figure S1–S8). The bulk purity was ascertained by elemental analysis. **2** in acetonitrile showed a structured spectrum in UV-Vis spectroscopy with absorption maxima at 295 and 398 nm followed by shoulders at 416 and 518 nm, which got relatively unstructured in water and PBS (Table 1 and Figure S6). Both the complexes exhibit green fluorescence with emission maxima of 508 (for **1**) and 516 nm (for **2**) with a low quantum yield of 0.002 and 0.0045 respectively in acetonitrile (Table 1 and Figure S5–S8).

Solution Stability

Ru polypyridyl complexes are mostly kinetically inert and stable under physiological conditions.[5,9] The stability of both complexes in solution was evaluated using reverse-phase high-performance liquid chromatography (RP-HPLC) in a 10 mM phosphate buffer with a pH of 7.4, containing 4 mM NaCl

Table 1. Photophysical properties of **1** and **2** with their corresponding ligands in acetonitrile.

	λ_{abs} (nm)	ε (dm^3mol^{-1} cm^{-1})	λ_{em} (λ_{abs}) (nm)	Stokes shift (nm)	Φ_f
1	296, 399, 416, 515		507(416)	91	0.002
2	295, 400, 416, 515	55680(295), 47050(400), 44070(416), 13230 (515)	518(416)	102	0.0045
Curcumin	418		538(418)	120	0.075
Morphocumin	420	57020	507(420)	87	0.081

(intracellular salt concentration), The HPLC analysis revealed that when dissolved in a DMSO : buffer mixture (4:6 v/v) at pH 7.4, a 400 μM stock solution of each complex remained stable for up to 48 h. Complex **1** eluted at 17.8 minutes and complex **2** at 12.3 minutes, with no new peaks detected during the 48 h period (Figures S9 and S10). This indicates that, in the absence of an external reagent to react with Ru(II) or the curcumin scaffold, both complexes are stable at physiological pH of 7.4. Additionally, the aqueous solubility and stability of complex **2** under physiological conditions were further examined using UV-Vis stability kinetics with a reduced DMSO concentration. A 50 μM solution of complex **2** in phosphate buffer at pH 7.4 containing 5% DMSO was monitored over 24 h via UV-Vis spectroscopy (Figure S11), confirming that **2** is stable in aqueous solution.

Cytotoxicity: Light vs. Dark

Over the past two decades, Ru polypyridyl complexes have gained recognition primarily in the field of photodynamic therapy.[9] Research indicates that *N,N*-coordinated Ru polypyridyls exhibit photodynamic properties, while *O,O*-coordinated ones are generally more suitable for chemotherapy rather than phototherapy due to their high dark toxicity, leading to a poor phototherapeutic index.[43] The present study focuses on a stable curcumin derivative, which is a photoactive chromophore capable of generating ROS when exposed to light. Consequently, we examined the light vs. dark cytotoxicity of *O,O*-coordinated curcumin and morphocumin-based Ru-bis-bipyridyl complexes. We employed three different protocols, well-documented in the literature, to assess phototoxicity (Table 2).[19,45] This approach provided evidence of the protocol that more accurately represented phototherapeutic vs. chemotherapeutic activity index of **1** and **2** (Table 2).

It is worth noting that all phototherapeutic experiments conducted utilized low light fluence (10 J/cm^2) since low fluence rates enhances the body's ability to fight tumors while also mitigating negative side effects.[46] Apparently it is found that the damage caused by lower PDT fluence rates tends to be lasting,[47] whereas higher irradiances can exhaust the oxygen supply in tumor tissues, resulting in less effective treatment.[46,48] Another advantage of using low-fluence irradiation is the diminished occurrence of photobleaching in photosensitizers during PDT treatment.[49] Thus, PDT administered at lower irradiances might prove more effective in preclinical trials. To measure chemotherapeutic activity, a standard and widely used protocol was followed.[50] The target cancer cells were representative of triple-negative breast carcinoma (MDA-MB-231) and human pancreatic carcinomas (MIA PaCa-2 and PANC-1) which are known to be difficult to cure. Data revealed that the morphocumin based **2** has a poor phototherapeutic index (PI > 3). **2** was found to be more toxic in the dark compared to its Ruthenium-*p*-cymene based half-sandwich congener, in MDA-MB-231 cells under a similar protocol (protocol 1). Albeit, **2** is more potent than the curcumin-based **1** irrespective of cell lines or protocols (Table 2 and Figures S12-S13).[19] The results demonstrated that variations in drug incubation time and cell recovery time after drug removal upon light/dark treatment lead to differences in IC_{50} values, evident from the phototherapeutic index (PI) shown in the comparison table (Table 2) (Figures S12–S17). The 24 h growth post cell seeding, followed by 4 h drug treatment, then washing away excess drug followed by 1 h dark treatment/light irradiation (λ = 400–800 nm, 2.7 mW cm^{-2}, total 10 J cm^{-2}) and finally 19 h incubation in the dark for recovery and growth (protocol 1) gave the best selectivity of light vs. dark toxicity with a PI value of 3.2–9.6 for **2**. The increase of incubation time in dark post external drug removal and irradiation gave an extensive downfall in terms of PI though the IC_{50} enhanced, as evident from protocol 2 (24 h growth post cell seeding was followed by 4 h drug treatment, then washing away excess drug followed by 1 h light irradiation/dark treatment and finally 44 h incubation in the dark for recovery and growth). The PI became the least when drug incubation time was further enhanced keeping the recovery time post drug removal almost same (protocol 3). The observed low PI and the trend in cytotoxicity under both dark and light conditions suggested that the complexes remain inside the cells and exert toxicity even without light exposure. The low differences in PI suggested that we may conduct further studies by using the chemotherapeutic cytotoxicity protocol (protocol 4, Table 2), exhibiting nanomolar IC_{50} concentration (Tables 2–3, Figure 2 and Figures S18–S19). However, the phototherapeutic activity does not allow the complexes to be in the medium for 72 h unlike protocol 4 in Table 2, rather the complexes stay only for 24 h maximum in the medium and then the medium is washed out and replaced with fresh medium without any drug. So, we kept the drug incubation time 24 h (Protocol 5, Supporting information) to evaluate the actual potency of the chemotherapeutic agents. **1** and **2**, their respective ligands, and CDDP as a standard were studied in the human embryonic kidney HEK293 and pancreatic adenocarcino-

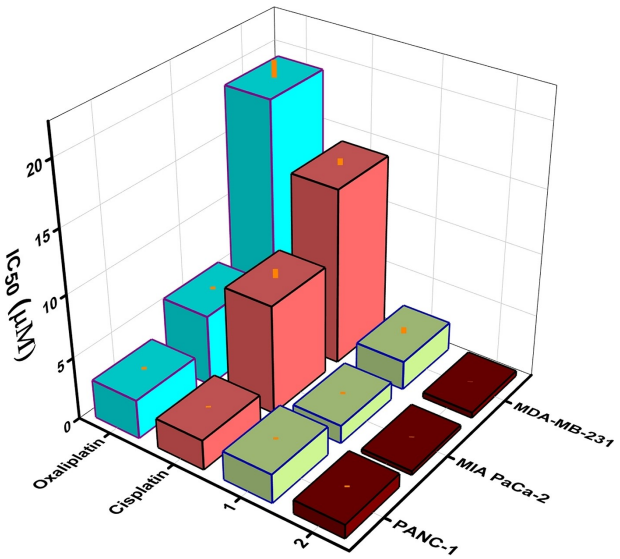

Figure 2. Comparison of *in vitro* IC_{50} for **1**, **2**, cisplatin and oxaliplatin in three different cancer cell lines showcasing the highest chemotherapeutic antiproliferative activity of the morphocumin based complex **2**.

Table 2. Comprehensive IC_{50} values (in μM) for **1** and **2** in different cancer cell lines in different protocols.

	IC50 ± SD[a] (μM)													
	Protocol 1: 24 h cell seeding → 4 h drug incubation → drug removal → 1 h photo/dark treatment in PBS → 19 h cell growth in dark				Protocol 2: 24 h cell seeding → 4 h drug incubation → drug removal → 1 h photo/dark treatment in PBS → 44 h cell growth in dark				Protocol 3: 24 h cell seeding → 24 h drug incubation → drug removal → 1 h photo/dark treatment in PBS → 48 h cell growth in dark				Protocol 4: 24 h cell seeding → 72 h drug incubation in dark	
Cell lines	Light		Dark		Light		Dark		Light		Dark		Dark	
MDA-MB-231	**1**	**2**	**1**	**2**	**1**	**2**	**1**	**2**	**1**	**2**	**1**	**2**	**1**	**2**
	>50	19.5 ± 2.4**	>50	62.3 ± 4.9**	4.7 ± 0.8**	4.4 ± 0.3**	>25	7.85 ± 0.2***	1.35 ± 0.2**	0.28 ± 0.02**	1.91 ± 0.16**	0.62 ± 0.02***	2.3 ± 0.5*	0.43 ± 0.01***
MIA PaCa-2	**1**	**2**	**1**	**2**	**1**	**2**	**1**	**2**	**1**	**2**	**1**	**2**	**1**	**2**
	>50	5.2 ± 1.2*	>50	>50	0.97 ± 0.07**	0.67 ± 0.06**	1.63 ± 0.5*	0.93 ± 0.18*	0.66 ± 0.06**	0.24 ± 0.01	1.59 ± 0.09***	0.38 ± 0.01***	1.43 ± 0.15**	0.30 ± 0.02**
PANC-1	**1**	**2**	**1**	**2**	**1**	**2**	**1**	**2**	**1**	**2**	**1**	**2**	**1**	**2**
	>50	16.8 ± 0.3***	>50	>50	2.93 ± 0.4**	2.8 ± 0.1***	4.9 ± 0.8**	4.9 ± 0.02***	1.3 ± 0.14**	0.73 ± 0.04**	3.7 ± 0.15**	1.1 ± 0.01***	2.3 ± 0.14**	1.1 ± 0.1**

[a] IC_{50} ± SD are determined by MTT (3-(4,5-dimethylthiazol-2-yl)-2,5-diphenyltetrazolium bromide) assay in normoxia (~15% O_2). The values show the ranges of two tailed P-values (One sample t-test, obtained from GraphPad Prism) corresponding to different levels of statistical significance. ns: $P > 0.05$, *: $0.01 \leq P < 0.05$, **: $0.001 < P < 0.01$ and ***: $P < 0.001$. The error bar shows standard deviation from three independent experiments. The error bar shows standard deviation from three independent experiments.

Table 3. Comparative chemotherapeutic IC_{50} (μM) values of **1** and **2** along with Cisplatin and Oxaliplatin.

	$IC_{50} \pm SD$[a] (μM)								
Complex	MDA-MB-231	TSI-1[b]	TSI-2[c]	MIA PaCa-2	TSI-1[b]	TSI-2[c]	PANC-1	TSI-1[b]	TSI-2[c]
1	2.3 ± 0.5*	6.1	8.3	1.43 ± 0.15**	6.1	3.98	2.3 ± 0.14**	1	1.3
2	0.43 ± 0.01***	32.8	44.7	0.30 ± 0.02**	29	19	1.1 ± 0.1**	2.2	2.8
Cisplatin	14.1 ± 0.5[50]			8.7 ± 0.7**			2.38 ± 0.1***		
Oxaliplatin	19.2 ± 1.2[51]					3.1 ± 0.2[52]			

[a] IC_{50} ± SD are determined by MTT assay in normoxia (~15% O_2). The values show the ranges of two tailed P-values (One sample t-test, obtained from GraphPad Prism) corresponding to different levels of statistical significance. ns: $P > 0.05$, *: $0.01 \leq P < 0.05$, **: $0.001 < P < 0.01$ and ***: $P < 0.001$. The error bar shows standard deviation from three independent experiments. The error bar shows standard deviation from three independent experiments. [b] TSI-1: therapeutic selectivity index-1: IC_{50} of Cisplatin/IC_{50} of the complex. [c] TSI-2: therapeutic selectivity index-2: IC_{50} of Oxaliplatin/IC_{50} of the complex

ma MIA PaCa-2, for comparison between a non- cancerous and cancerous cell line. We found that whether the drug is incubated in the medium for 24 or 72 h the IC_{50} remained almost the same (Table S1). Furthermore, all the examined complexes were discovered to be equally toxic, if not more so, in HEK293 than in MIA PaCa-2, indicating their non-specificity (Table S1, Figures S20–S21). In addition this also depicts that unlike the Pt drugs cisplatin and oxaliplatin the complexes are not susceptible to sequestration by ATP7 A which is highly populated in HEK293.[53]

Electrostatic Potential Maps

The cause of exhibition of poor phototherapeutic activity of *O,O*-coordinated ruthenium polypyridyl complexes is suggested to be due to the LUMO (lowest unoccupied molecular orbital) of such Ru(II) complexes having minimal or no contribution from the Ru–O σ* orbitals. So even under photoirradiation, the Ru–O σ* orbitals remains largely unoccupied in the excited state, thus preventing the release of the ligand for PACT type activity.[54] We initially conducted density functional theory (DFT) calculations (B3LYP/6-31G(d,p)) with water as the solvent (defined by the IEFPCM model) to determine the electrostatic potential surfaces (ESP) of **1** and **2**. In Figure S22, the light blue area of the complexes housing the curcumin or morphocumin scaffold, demonstrates high electron density, while the intense blue region corresponding to the bipyridine motif exhibits reduced electron density. Both complexes exhibit similar ESP profiles.

Analysis of the frontier molecular orbitals and the natural transition orbitals corresponding to our predicted UV-Vis spectra, utilizing the PM6 semi-empirical model, gave the best fit to the experimentally determined spectra (Figure S23) and the electron-hole pairs. The calculation reveals that the HOMO (highest occupied molecular orbital) is predominantly localized on the curcumin/morphocumin, while the LUMO is centered on the bipyridyl group (Figure S24 and Tables S2–S5). The HOMO-LUMO bandgap for both **1** and **2** is comparable, and there is minimal contribution from Ru–O σ* orbitals in the LUMO, aligning with the literature findings. Consequently, no photo-release of curcumin or morphocumin from **1** and **2** respectively, was observed upon irradiation with visible light. Analyzing the Natural Transition Orbitals (NTOs) for **2** predicted at 511.8 and 534.8 nm (corresponding to the peak on the spectra), it was observed that the electron-hole pair transitions do not end up populating the Ru–O σ* orbitals, and hence, no ligand dissociation upon photoirradiation (Table S5).

Stability Comparison upon Various Stimuli Responses

pH stability: The stability of complexes in endosomal pH 5 through reverse phase HPLC revealed that both the complexes were intact in phosphate buffer of pH 5 containing 4 mM NaCl up to 24 h (Figure 3a and Figures S25–S26). In our previous work, the [Ru^{II}(*p*-cymene)(morphocumin)Cl] also showed excellent stability in acidic pH.[19] Thus, replacing the arene motif with bipyridyl did not alter the stability of these complexes. This signifies that if the complexes are internalized by endocytosis, then in the endosome the complexes remain intact for release inside cells.

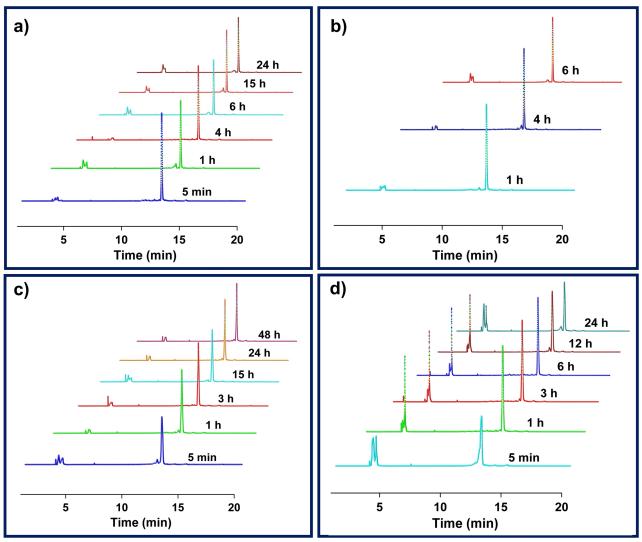

Figure 3. RP-HPLC chromatogram of **2** in 4:6 v/v DMSO and phosphate buffer (10 mM phosphate, 4 mM NaCl) with respect to time under various conditions. a) Stability at pH 5 up to 24 h. b) Stability upon photo-irradiation (λ = 400–800 nm, 2.7 mW cm^{-2}; total 10 J cm^{-2}) up to 6 h. c) In the presence of 10 equiv. GSH up to 48 h. d) In presence of 5 equiv. 9-EtG up to 24 h.

Photostability: Photostability of the complexes were investigated through UV-Vis as well as HPLC. 25 μM of each **1** and **2** in acetonitrile was irradiated with visible light (λ = 400–800 nm, 2.7 mW cm^{-2}, total 10 J cm^{-2}) for 1 h (similar dose used for *in vitro* PDT) but their UV-Vis spectra remained almost unaltered revealing their stability upon irradiation (Figures S27 and S28). A similar experiment conducted by HPLC by incubating the complexes in 4:6 v/v DMSO and phosphate buffer of pH 7.4 containing 4 mM NaCl (Figure 3b and Figures S29–S30) showed that even up to 6 h post-irradiation (hpi) there is no photodissociation, as no new peak generated in the HPLC chromatograms.

Stability against Glutathione and 9-EtG binding: Cancer cells generate resistance to chemotherapy by metal complexes of Ru/Pt/Ir by increasing the population of soft donors like glutathione (GSH) exploiting the HSAB principle. GSH has a wide-ranging spectrum of action and extensive distribution because of its solubility in both water and lipids. GSH binding to a drug helps to efflux it out of the cell by active transport, a pathway of chemotherapy resistance.[55] Hence kinetic inertness is an important property to fight the sequestration by soft donors like GSH and other thiol donor based sequestration /transport proteins. Reverse phase HPLC showed no GSH bound peak for **1** and **2** up to 48 h when 10 equiv. of GSH was co-incubated with respective complexes using buffer of pH 7.4 (Figure 3c and Figures S31–S32). The coordinative saturation and tight binding may be the reason for the stability. This stability also makes it non-reactive towards the model nucleobase 9-Ethtylguanine (9-EtG). Even 5 equiv. of 9-EtG to **1** or **2** at pH 7.4 showed no adduct formation (Figure 3d and Figures S33–S34). The above data suggests that the intact complexes are active agents without needing to dissociate and dissociation of the bidentate morphocumin would widen the target domain for **2**, since morphocumin is stable inside cell, targets lysosome and is also photoactive.

H_2O_2 mediated ligand release: Several human carcinoma cell lines produce significant amounts of hydrogen peroxide (H_2O_2) in vitro without external stimulation at a significant rate unlike most normal cells. The elevated amount of H_2O_2, the most chemically stable ROS in tumor microenvironment compared to normal cells is often utilized as responsive stimuli for prodrug activation or therapeutic ligand release.[56,57] A solution of the complexes and various equivalents of H_2O_2 (200, 500, and 1000 equiv. respectively) at 37 °C was used to investigate the time-dependent stability of **1** and **2** by reverse phase HPLC (Figures S35–S40). Ligand release was evident for **2** (Figure 4a) but **1** dissociates to several species. Incubation of **2** with 200 equiv. H_2O_2, showed a slow release of morphocumin which increased from 14 % → 22 %→ 32 % after 24 h, 48 h, and 72 h respectively (Figure 4b, c and Figure S36). When the amount of H_2O_2 was elevated to 500 equiv, the percentage of released morphocumin enhanced up to 21 % and 36 % after 24 h and 48 h, respectively (Figure 4a and Figure S38). Upon incubating with 1000 equiv. H_2O_2, more than 50 % morphocumin released within 12 h but the morphocumin also oxidized or degraded (Figure 4a and Figure S40). It is worth mentioning that there was no auxiliary addition of H_2O_2 during the time-dependent studies, while in tumor microenvironments continuous production of H_2O_2 takes place.[22] Strikingly, under similar conditions, **1** did not release curcumin except when the H_2O_2 concentration was enhanced to 1000 times and then the complex dissociate to many uncharacterized species. Since the stability of curcumin is much poorer in the presence of ROS compared to a normal physiological condition, it can be assumed that even if it is released from **1**, it would degrade. This is supported by our HPLC stability data of standalone curcumin recorded under similar concentrations of H_2O_2 (Figure S41). The stability of morphocumin was scrutinized in presence of 200 equiv. H_2O_2 up to 24 h and it is mostly stable (Figure S42), unlike curcumin. So, **2** is also advantageous from the perspective of releasing morphocumin, a lysosome targeting PDT agent with much higher stability than curcumin in the harsh environment of cancer cells. Previously, different research groups have reported stimuli responsive release of curcumin derivatives from metal complexes as summarized in Table S6. The data shows that curcumin is released from metal complexes of Pt(II), Co(III) and Fe(II/III) using stimuli like visible light, GSH, ascorbic acid but not H_2O_2 which is continuously produced in cancer cells in cancer cells.

GSH based release of ligand for a metal complex may be disadvantageous since when a metal complex releases curcumin in the presence of excess GSH that suggests that the metal complex is now a potential binding site for the GSH if the metal is relatively soft electrophilic centre, thus disrupting the mechanism of action, which is not the case with our complex

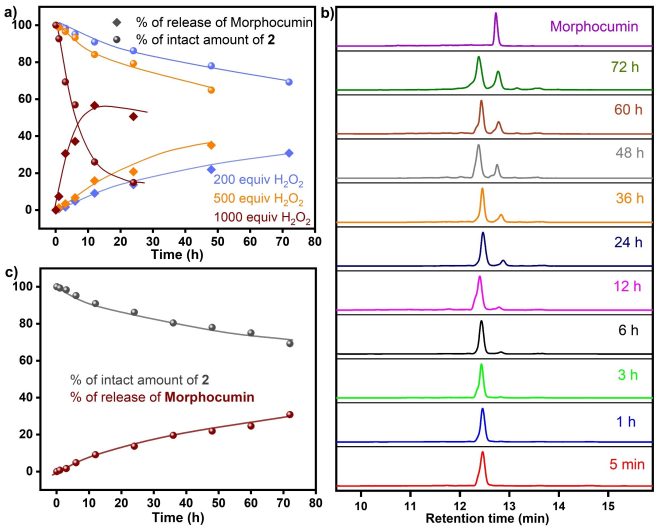

Figure 4. H_2O_2 mediated ligand release from **2**. a) Cumulative plot of release of morphocumin from **2** in the presence of 200, 500 and 1000 equivalent H_2O_2. Y-axis denotes the % of intact amount of **2** and Morphocumin (calculated from area under the peak in respective HPLC chromatograms), X-axis denotes different time points of experiments. Solid lines are a guide to eye. b) RP-HPLC chromatogram of **2** in 4:6 v/v DMSO and phosphate buffer (10 mM phosphate, 4 mM NaCl, pH 7.4) in the presence of 200 equiv. of H_2O_2 up to 72 h showing increase in release of morphocumin from **2** with respect to time. c) Plot of time-dependent morphocumin release from **2** in the presence of 200 equiv. H_2O_2 by taking the area under the respective HPLC chromatogram from (b). Y-axis denotes the % of intact amount of **2** and morphocumin, while X-axis denotes different time points of experiments. Solid lines are a guide to eye.

since **2** shows significant resistance to excess GSH. The reactivity of **2** towards H_2O_2 to release morphocumin which unlike curcumin is stable in the ROS rich environment and also a phototherapeutically active compound under visible light irradiation makes **2** unique from its predecessors. In addition, the required dose for chemotherapeutic activity of these *O,O*-coordinated complex is also better than the earlier reported complexes depicted in Table S6.

Determination of ROS Generation and Type of Photo-process

The indication that **2** releases the stable morphocumin in the presence of hydrogen peroxide led us to evaluate the potential of **1** and **2** in generation of ROS. We select two distinct ROS indicators for each of the two potential photo-process types. The absorbance of 9,10-anthracenediyl-bis(methylene) dimalonic acid (ABDA), a known $^1O_2$ specific indicator, did not decrease upon exposure of **1** or **2** to visible light (400–800 nm, 2.7 mW cm^{-2}), confirming non-involvement of type II photo-process (Figure S43). Previously, **1** was shown to proceed via type-I pathway generating ROS other than $^1O_2$ but the exact ROS involved remains unknown.[43] We find that **1** and **2** produce hydroxyl radicals, a specific class of type I ROS, when exposed to photo-irradiation in PBS (5% DMF) using a standard spectroscopic method that depends on the OH oxidation process turning the non-fluorescent HPF probe fluorescent.[58] The data (Figure S44) suggests OH radical (ȮH) generation by **2** upon photo-irradiation. The results obtained with **1** and **2** are similar as both proceed via type-I pathway promoting the generation of ROS through electron transfer. At only 1 μM dose both **1** and **2** generate ROS inside MDA-MB-231 cells converting the non-fluorescent DCFDA to fluorescent DCF (Figure S45) suggesting the *O,O* donor curcumin and morphocumin as a ligand are equally efficient in generating ROS but the disadvantage of curcumin is its instability in the presence of ROS unlike morphocumin, which is highly stable as discussed earlier.

Capacity Factor, Lipophilicity and Cellular Accumulation

The lipophilicity and cellular accumulation provide relevant information of drug-like properties. Lipophilicity of complexes **1** and **2**, determined using reverse-phase high-performance liquid chromatography (RP-HPLC) showed that the capacity factor (k) values, which reflect the retention of compounds in the chromatographic system is higher for **1** (k = 4.42) than **2** (k = 0.18), indicating greater lipophilicity for **1**. Comparison with free curcumin (k = 5.98) and morphocumin (k = 0.26) revealed that the ligands contribute significantly to the hydrophobicity or hydrophilicity of the complexes (Figure 5a). The lower capacity factor of the corresponding complexes suggests that the Ru-bis-bipyridyl promotes hydrophilicity. Given that there is a well-established linear relationship between log(k) and log ($P_{o/w}$),[59] we calibrated our system using the six reference chemicals listed in the OECD guidelines: 1-Naphthol, Benzophenone, Phenanthrene, Diphenyl Ether, and Naphthalene. Upon fitting with a straight line (Figure S46), the equation obtained for the system (1:1 MeCN: H_2O) is found to be:

$$\log(P_{o/w}) = 1.90416 \bullet \log(k) + 1.82532;\ R^2 = 0.946$$

The calculated lipophilicity shows a higher lipophilic character of **1** compared to **2** (Table 4) in accordance with the trend in k values. Treatment of MIA PaCa-2 cells with equimolar concentrations (10 μM) of **1** and **2** for 6 h and analysis by Inductively Coupled Plasma Optical Emission Spectroscopy (ICP-OES) showed higher cellular accumulation of **2** (almost 1.4-fold

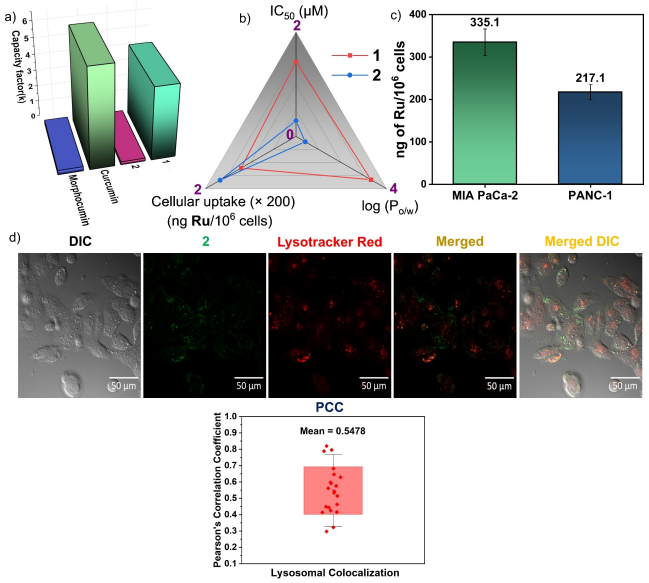

Figure 5. a) Capacity factors (k) of **1** and **2** with their corresponding ligands. b) Correlation diagram of IC_{50} (in MIA PaCa-2 cells), Log P and cellular uptake (in MIA PaCa-2 cells) for **1** and **2**. c) Comparative plot of cellular uptake for **2** in MIA PaCa-2 and PANC-1 cell lines. d) Lysosomal colocalization of 10 μM of **2** in MDA-MB-231 cells using lysotracker Red DND-99 (200 nM) for observing co-localization along with calculated Pearson's correlation coefficient (PCC) value.

Table 4. Chemotherapeutic IC_{50}, lipophilicity and cellular uptake of **1** and **2** with their corresponding ligands.

Complexes	IC_{50} in MIA PaCa-2 cells (μM) [72 h drug incubation]	LogP	Uptake in MIA PaCa-2 cells (ng/mol)
1	1.43 ± 0.15	3.054	242.5 ± 21
2	0.3 ± 0.02	0.407	335.1 ± 31
Curcumin	6.15 ± 0.2	3.304	ND
Morphocumin	6.8 ± 0.2	0.711	ND

higher than **1**) (Table 4). The internalization data correlates well with the cytotoxicity profile, but it is important to note that there is no linear correlation between lipophilicity, cellular uptake and cytotoxicity for **1** and **2** (Figure 5b). Based on the cytotoxicity profile, to ascertain if the better IC_{50} values were due to higher cellular uptake, we performed ICP-OES for **2** in PANC-1, in which the complex was found to be the least potent among three tested cell lines. The data suggested that cellular uptake in PANC-1 cells is 1.5-fold lesser for **2** than that in MIA PaCa-2 cells under similar conditions, which may be one of the major reasons for **2** showing better efficacy in MIA PaCa-2 over PANC-1. (Figure 5c). This also suggested that if we can improve uptake and selectivity then the potency of the complexes would be increased (*vide infra*). Our next step was to find if **2** also have co-localization in lysosome since that would further elucidate if the cells were killed via lysosome degradation due to ROS generation inside lysosomes

Subcellular Colocalization and DNA Interaction Study

Morphocumin mostly localize in lysosome (Pearson's correlation coefficient (PCC) = 0.85) and so does the Ru-*p*-cymene complex (PCC = 0.65) as shown by us earlier.[19] Complex **2** however, is at least 17 fold more active in MDA-MB-231 cells but unlike the Ru-*p*-cymene-Cl congener shows lower lysosomal co-localization by confocal microscopy (PCC = 0.54) (Figure 5d). Thus, the non-organometallic bis-bipyridyl motif conjugation with Ru(II) incorporates alteration in the organelle targeting ability. The amount of **2** accumulating in lysosome may still enable lysosomal disruption leading to cell death by autophagy or apoptosis.

Ru(II) polypyridyl complexes and curcumin derivatives have shown affinity towards DNA.[60] Previously, Ru bis-bipyridyl curcumin complex (**1**) and its analogs were found to be DNA groove-binders.[43,61] This information guided us to investigate nuclear localization of complex **2**. In MDA-MB-231 cell line, the result shows a marginal localization of **2** in nucleus (PCC = 0.27) (Figure S47). The nuclear colocalization is minimal; however, we still conducted DNA interaction studies to determine if there is a possibility of interaction. Since Ru polypyridyl complexes and Ru-polypyridyl-curcumin scaffolds are reported for binding with DNA through multiple interaction modes.[4,44,61]

1 and **2** showed hypochromism of calf thymus DNA absorption indicating interaction between the complex's electronic states and the stacked DNA base pairs (Figure S48a-b). This may be because the partially filled π^* orbital of **1** and **2** comes in proximity with the DNA's π orbitals, lowering transition probabilities, evidenced by hypochromism.[62] Fluorescence intensity of **2** also increased upon sequential addition of CT-DNA addition suggests that interaction with DNA may be restricting the free rotation of **2** in solution, enhancing the fluorescence (Figure S48c).[62] However, it must be noted that **2** co-localizes more in lysosome than in nucleus and in presence of ROS, **2** would release morphocumin in cell and the released morphocumin is known to localize highly in lysosome.[19] Hence the DNA binding mode may be a minor pathway of action for **2**.

Studying the Mechanism of Action in the Presence of Inhibitors

Our studies so far highlighted that whether we use protocol 4 or 5 for chemotherapeutic activity the results will be similar. The studies also suggest that protocol 3 may be the best choice for measuring phototherapeutic activity in similar systems. The indication from the above studies suggested that cellular uptake as well as cytotoxicity profile of **2** is excellent in MIA PaCa-2 cell line. We thus investigated the chemotherapeutic mechanism of action of **2** in MIA PaCa-2 cell line by using various inhibitors. Since the bidentate active ligand in **2**, is the lysosome targeting morphocumin,[19] so we used Leupeptin, a known lysosomal protease inhibitor, well-documented to curb the activity of lysosomal hydrolase and prevent lysosome-mediated cell death[63] by inhibiting cysteine, serine, and threonine proteases.[64] The cell viability of **2** co-incubated with 10 μM Leupeptin gave no difference in the IC_{50} values (Figure 6a, Figure S50), ideally suggesting that the cell death rendered by the complexes are not affected by the inhibition of lysosomal hydrolases. In contrast, there is almost 1.5-fold reduction in IC_{50} of morphocumin by co-incubation with 10 μM leupeptin suggesting that free morphocumin promotes lysosome-mediated cell death (Figure S51). Thus, complex formation changes the pathway of action with respect to the free

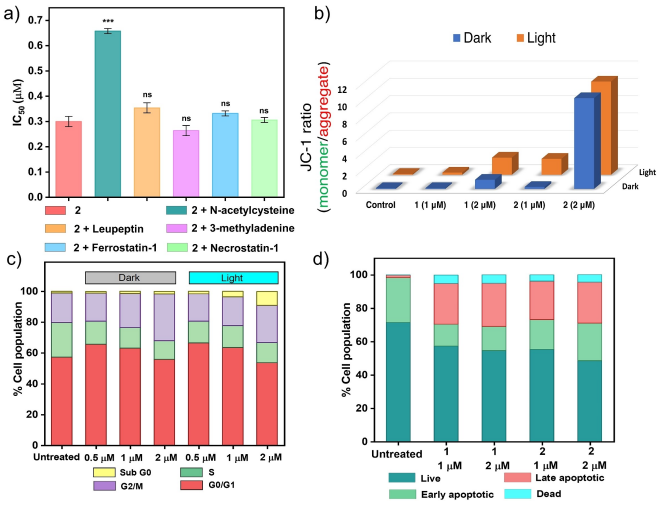

Figure 6. a) Cytotoxicity of **2** in MIA PaCa-2 cell line in presence of various inhibitors, Leupeptin (10 μM) as lysosomal protease inhibitor; *N*-acetylcysteine (5 mM) as ROS suppressor; 3-methyl adenine (100 μM) as autophagy inhibitor; Ferrostatin-1 (60 μM) as Ferroptosis inhibitor; Necrostatin-1 (60 μM) as Necroptosis inhibitor. The figure shows the ranges of P-values (Two sample t-test) corresponding to different levels of statistical significance. ns: $P > 0.05$, *: $0.01 \leq P < 0.05$, **: $0.001 < P < 0.01$ and ***: $P < 0.001$. The error bar shows standard deviation from three independent experiments. b) Change in mitochondrial membrane potential upon 24 h treatment of **1** and **2** (1 and 2 μM) in light and dark. c) Cell cycle phase arrest of **2** (0.5, 1, 2 μM for 24 h) in light and dark. d) Induction of apoptosis by **1** and **2** (1 and 2 μM for 24 h) in chemotherapeutically in MIA PaCa-2 cell lines as analyzed through Flow cytometry.

morphocumin. Complex **2** also does not kill by autophagy as indicated by the unchanged IC_{50} values in presence of 100 μM of standard autophagy inhibitor 3-methyladenine (Figure 6a and Figure S50). The IC_{50} of **2** also did not change in presence of 60 μM of each Ferrostatin-1 and Necrostatin-1 suggesting Ferroptosis or necroptosis respectively are not involved in cell death (Figure 6a and Figure S50).

The intracellular ROS generation study reveals the potential of **2** to induce ROS irrespective of light or dark. So, the cytotoxicity of **2** was investigated in the presence of *N*-acetylcysteine (NAC), a well-known ROS inhibitor and suppressor. **2** co-incubated with 5 mM NAC gave two-fold poor IC_{50} (Figure 6a and Figure S50). NAC plays a significant role in reducing oxidative stress by scavenging ROS like, peroxide and hydroxyl radicals to prevent cellular damage. It also promotes glutathione synthesis, mitochondrial protection and prevent apoptosis induced by oxidative stress.[65] Thus, co-incubating **2** with NAC leading to poor IC_{50} suggests a possible role of **2** in inducing oxidative stress through ROS generation.

Investigating the Mechanism of Action: Cyclic Voltammetry, NAD^+ Interaction, JC-1, Cell Cycle Arrest and Apoptosis

A compound may help accumulation of ROS in several ways which include disrupting the mitochondrial function or reacting with the molecular oxygen in cells. The complex may be redox active in cellular conditions. Thus, we investigated **2** for redox activity in dark. The data showed that the oxidation potential of **2** in acetonitrile is 0.47 V vs. SCE (0.07 V vs. Ferrocene; 0.71 V vs. NHE) (Figure S52). It is suggested that Ru-polypyridyl complexes having redox potential value in the range of 0.4–0.6 V vs. SCE are found to be most cytotoxic.[66] The value of redox potential of **2** with respect to NHE is close to the biological range of ±0.5 V.[67] The ability of **1** and **2** to catalyze the reduction of NAD^+ to NADH was scrutinized in the presence of formate as a hydride donor.[68] Both **1** and **2** (2 μM) co-incubated with NAD^+ (100 μM) in the presence of formate (300 μM) showed no reduction of absorbance at λ_{340} nm excluding the possibility of NAD^+ reduction to NADH (Figure S53) by **2**.

Next, we looked into the possible change of mitochondrial membrane potential since **2** show accumulation of ROS which may be due to disruption of the mitochondrial function. During the course of several different cell death modes, an event that begins promptly is the depolarization of the mitochondrial membrane potential (MMP). MIA PaCa-2 cells were treated with 1 μM and 2 μM dose of both **1** and **2** in the presence as well as absence of photo-stimuli. Significant dose dependent and stimuli dependent depolarization of MMP by **1** and **2**, showed elevation of JC-1 monomer's green emission intensity compared to the red emitting aggregates present in healthy mitochondria. Both **1** and **2** induced greater depolarization of MMP upon photo-irradiation compared to dark condition and **2** exhibited pronounced effectivity in all cases compared to **1** (Figure 6b and Figure S54).

Then, the cell cycle analysis in MIA PaCa-2 cells were performed to know if there is arrest in any particular phase of the cell cycle. MIA PaCa-2 cells were treated with various doses of **1** and **2** in the presence and absence of light. Both **1** and **2** exhibit arrest in Sub G0 phase upon photo-irradiation while interfering with the G2/M phase in dark (Figure 6c and Figures S55–S56). There are several factors which may influence the arrest of cell cycles by a compound, one of them is certainly the specificity and toxicity of the drug. Drugs that arrest in Sub G0 phase may be more selective for cancer cells and can spare normal cells that are in the resting state, as they can target cells that have abnormal signals or damages.[69] On the other hand, drugs that arrest in G2/M phase may affect both cancer and normal cells, as they can interfere with the normal cell cycle.[69,70] It is also reported for several photoactive drugs to have different cell cycle phase arrest in the presence and absence of light.[71] However, in our case, such differences were not anticipated, since we observed minimal alteration in dose response in the presence and absence of light. However, the cell cycle arrest and the mitochondrial depolarization data suggest that in spite of the toxicity dosage being similar in the presence and absence of light there exists a difference in pathway of action.

Annexin-V PE and 7AAD were used in the cell death assay, which demonstrated that both **1** and **2** cause apoptosis in a dose-dependent manner (Figure 6d and Figure S57). Accordingly, our findings imply that the ROS produced by the complexes kill through the intrinsic mechanism of apoptosis mediated by the mitochondria.

Encapsulation in Glucose Functionalized Polymeric Nanoparticles

One of the hallmarks of pancreatic ductal adenocarcinoma (PDAC) is dramatically enhanced glycolytic flux, characterized by 'Warburg effect', and this is also true for many other cancers.[72] In similarity with many other cancers, in PDACs to fulfill the requirement of glucose and its transport across plasma membrane GLUT1, also known as solute carrier family 2 facilitated glucose transporter member 1 (SLC2 A1), is overexpressed.[73,74] Studies analyzing GLUT-1 expression in 53 pancreatic cancer tissues found that overexpression of GLUT-1 was associated with poor prognosis and adverse clinicopathological features, including increased tumor size, higher maximum standardized uptake value (SUV_{max}), lymph node metastasis, advanced clinical stage, and elevated Ki-67 expression.[74,75] In spite of the excellent cytotoxicity, **2** displays low chemotherapeutic selectivity index (IC_{50} in normal cell/IC_{50} in cancer cell) thus to enhance selectivity and make delivery more feasible we employ a glucose conjugated polymer with the capacity to form micelles that encapsulate and deliver **2** more selectively to cancer cells.[40,41]

We noted that establishing a suitable interaction between the glucose units of the polymer and GLUTs is feasible when the polymeric nanocarriers are structured in a manner that ensures the retention of glucose segments within their outer shell. Moreover, to attain optimal drug encapsulation within the nanocarriers, it is imperative to have balanced hydrophilic and

hydrophobic segment in the polymer. Therefore, a glucose-based polymer was synthesized utilizing the reversible addition-fragmentation chain-transfer (RAFT) polymerization technique, ensuring controlled chain growth and precise incorporation of hydrophobic and hydrophilic segments within the polymer.

Initially, the glucose-based monomer Ac–G-EMA (Figure 7a and Figure S58) was synthesized according to previous literature[76] using β-D-glucose pentaacetate and 2-hydroxyethyl methacrylate (HEMA). The Ac–G-EMA was then copolymerized with hydrophobic methyl methacrylate (MMA) *via* the RAFT polymerization method, employing 4-cyno-4-(dodecylsulfanylthiocarbonyl) (CDP) as the chain-transfer agent (CTA) and 2,2-azobisisobutyronitrile (AIBN) as the initiator. During the polymerization, the molar ratio of [Ac–G-EMA]/[MMA]/[CDP]/[AIBN] was maintained as 20/10/1/0.1 (Figure S59). The resulting copolymer, P(Ac–G-EMA-*co*-MMA), was characterized by using ^{1}H NMR and size exclusion chromatography (SEC) analysis. The number average molecular weight ($M_{n,NMR}$) of the polymer was calculated from NMR analysis with respect to the end-group protons (COOHCH_2CH_2–) of CDP at 2.4–2.6 ppm, yielding a value of 8000 g/mol. This value is in close agreement with the theoretical molecular weight ($M_{n,theo}$), which was calculated using the following equation: $M_{n,theo}$ = (([monomer]/[CDP] × average molar mass of monomer × conv.) + (molar mass of CDP)). SEC analysis provided the number average molecular weight ($M_{n,SEC}$) and dispersity ($Đ$) of the polymer, with poly(methyl methacrylate) (PMMA) as a standard (Figure S60). The polymer's characterization is summarized in Table S7. Finally, the acetyl groups of P(Ac–G-EMA-*co*-MMA) were deprotected to yield the desired glucose-conjugated copolymer (**DP**) (Figure 7a and Figure S59). In an aqueous medium, the micellization of **DP** was confirmed through critical aggregation concentration (CAC) measurement and dynamic light scattering (DLS) studies. The CAC of **DP**, determined using Nile red (NR) as a hydrophobic fluorescent probe[77] is approximately 30.1 μg/mL in aqueous medium (Figure 7b). Additionally, the morphology of these micelles was further validated by field emission scanning electron microscopy (FESEM) and transmission electron microscopy (TEM) analyses, with the estimated sizes of **DP** from TEM and FESEM images being 76.1 ± 9.8 nm and 71.5 ± 15.3 nm, respectively.

Once the glucose-based copolymer was synthesized, we proceeded to encapsulate complex **2** in **DP** to create drug-loaded glucose-based nanoparticles, labeled **DP@2**. We calculated the drug loading efficiency (DLE) and drug loading content (DLC) of the nanoparticles,[78] finding them to be 46.7% and 7.0%, respectively. Notably, the inclusion of **2** in **DP** did not alter the hydrodynamic diameter (D_h) as measured in PBS, with **DP** and **DP@2** showing D_h values of 82.9 ± 7.2 nm (PDI 0.599) and 75.2 ± 6.2 nm (PDI 0.635), respectively (Figure 7c). To further investigate the morphology of **DP@2**, TEM and FESEM analyses were conducted, revealing sizes of 88.2 ± 5.2 nm and 64.2 ± 13.2 nm, respectively (Figure 7d–g). The SEM-EDS spectrum of **DP@2** confirms the metal complex encapsulation (Figure S61). It is well-known that micelles smaller than 100–150 nm are less likely to be cleared by the reticuloendothelial system, making them suitable for drug delivery applications.[79,80] Therefore, we examined the efficacy of **DP@2** in cancer therapy, given its ability to release **2** within the cellular environment through esterase-mediated micellar degradation.

To exploit the altered metabolism of cancer cells characterized by accelerated glycolysis (Figure 8a), we assessed the cytotoxicity of **DP** and **DP@2** in MIA PaCa-2 and HEK 293 cell lines. Results showed that **DP** is non-toxic at doses up to 0.5 mg/mL in both cell lines (Figure S62). We also evaluated the IC_{50} values after a 24 h treatment to gauge the true effective-

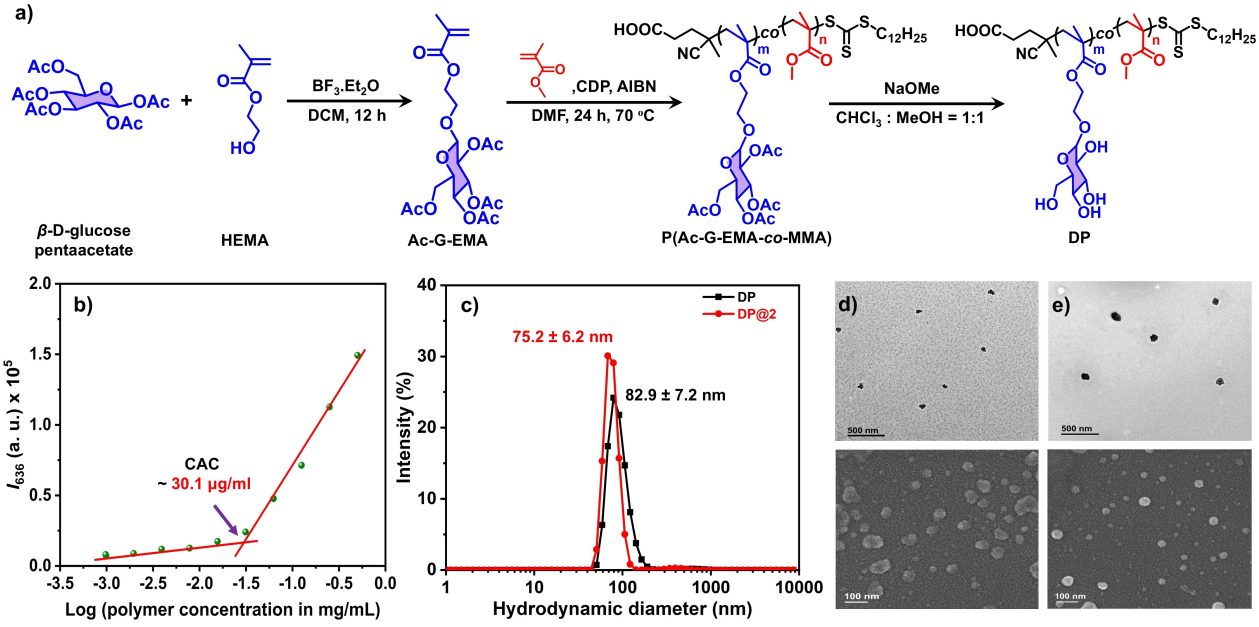

Figure 7. a) Schematic representation of synthesis of Ac–G-EMA, P(Ac–G-EMA-*co*-MMA) and **DP**. b) CAC plot of **DP** in water; c) DLS plot of **DP** and **DP@2** in PBS; TEM images of d) **DP** and e) **DP@2**. Scale bar = 500 nm; FESEM images of f) **DP** and g) **DP@2**. Scale bar = 100 nm.

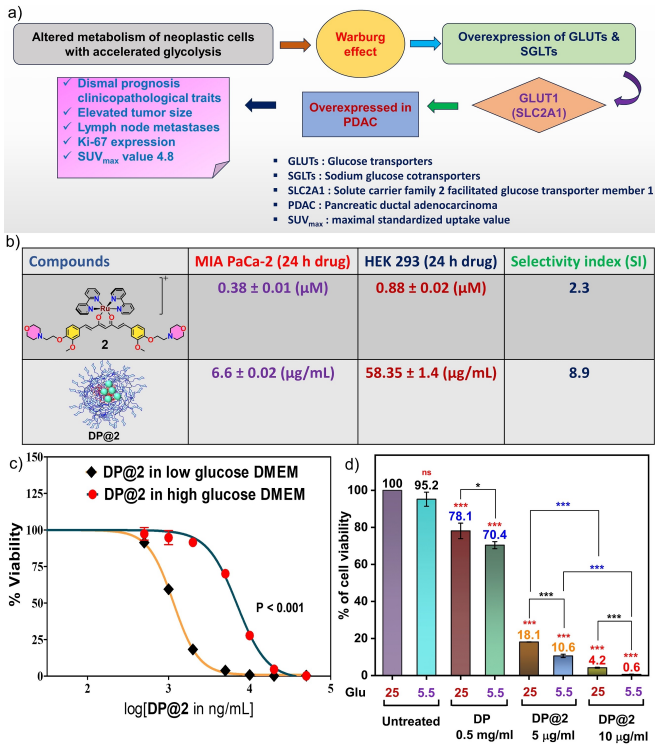

Figure 8. a) Schematic representation of Warburg effect and its consequences in pancreatic cancer. b) Enhancement of cancer selectivity upon encapsulation: IC_{50} of **2** and **DP@2** in MIA PaCa-2 and HEK 293 cell lines cultured in high glucose (25 mM) medium following protocol 5 (24 h drug incubation followed by drug removal and 48 h further incubation). c) Comparative cytotoxicity plot of **DP@2** in MIA PaCa-2 cells culturing in high (25 mM) and low (5.5 mM) glucose DMEM culture medium. Cytotoxicity is done by following protocol 5. $IC_{50} \pm$ SD are determined by MTT assay in normoxia (~15% O2). The statistical significance (P) of the data is < 0.001. The error bar shows standard deviation from three independent experiments. d) Cumulative bar diagram of % of MIA PaCa-2 cell viability for **DP** and **DP@2** as well as untreated control in high (25 mM) and low (5.5 mM) glucose medium. Each experiment was done in triplicate. The figure shows the ranges of p-values corresponding to different levels of statistical significance. ns: $P > 0.05$, *: $0.01 \leq P < 0.05$, **: $0.001 < P < 0.01$ and ***: $P < 0.001$. The error bar shows standard deviation from three independent experiments.

ness of chemotherapy. **DP@2** exhibited an IC_{50} of 6.6 ± 0.02 μg/mL in MIA PaCa-2 cells, while in HEK 293 cells, the IC_{50} was 58.35 ± 1.4 μg/mL, demonstrating nearly a 9-fold selectivity for cancer cells (Figure 8b and Figure S63).

To further understand the role of glucose-functionalized polymeric encapsulation, we examined the receptor-mediated engulfment efficiency of **DP@2**. We prepared DMEM medium with low glucose content. Typically, the standard DMEM culture medium contains a high glucose concentration of 25 mM. In this study, we determined the chemotherapeutic IC_{50} values of **DP** and **DP@2** by culturing them in a low glucose (5.5 mM) medium. Since cancer cells have a high demand for glucose, culturing them in glucose-deprived medium should prompt glucose-functionalized **DP** or encapsulated **DP@2** to enter the cancer cells *via* glucose receptors through endocytosis to meet their glucose requirements. As expected, the IC_{50} of **DP@2** decreased to 1.2 ± 0.04 μg/mL, which is 5.5 times more effective than its IC_{50} in high glucose medium under similar conditions (Figures 8d and Figure S63). In order for the above conclusion to be concrete we needed to ensure that low glucose concentration does not significantly alter cell survival. Thus, we carried out a control study varying glucose concentration with no drug, with **DP** (0.5 mg/mL) and **DP@2** (5 μg/mL and 10 μg/mL). The 72 h treatment study confirmed that cell survival is similar in both high and low glucose media (Figure 8c) and due to higher uptake taking higher amount of **DP@2** enhances killing ratio.

Conclusions

The study highlights the effectiveness of a Ru(II) bis-bipyridyl morphocumin complex (**2**) encapsulated within a glycopolymer, termed as **DP@2**, which exhibits high selectivity towards various cancer cell lines compared to non-cancerous HEK 293 cells. Complex **2** shows significant chemotherapeutic potential, particularly against the PDAC, MIA PaCa-2 as evidenced by its low IC_{50} value of approximately 300 nM. Noteworthy drug-like properties of **2** include its stability under physiological and endosomal pH conditions, as well as its stability under visible light and in the presence of glutathione. The high selectivity of the **DP@2** delivery assembly suggests that these non-selective yet highly efficient Ru(II) polypyridyl complexes can be molded into selective and effective promising chemotherapeutic agents. Our detailed protocol analysis for phototherapy vs. chemotherapy assays advises caution in using the proper protocol for phototherapy (e.g., Protocol 3) to accurately distinguish their activity from observed dark toxicity across various cell lines. The morphocumin release in presence of excess H_2O_2 and enhancement of reactive oxygen species (ROS) by **2** inside cellular environment suggest a possible synergistic domino effect releasing more morphocumin bringing in multiple pathways of action *via* lysosome and mitochondrial function disruption to induce apoptotic cell death. The suitability of the glycopolymer as a delivery vehicle due to excellent loading of **2** suggests a good compatibility between the **DP** and **2**. Importantly, the proof-of-concept for selectivity is shown through glucose functionalization, enhancing selectivity by approximately 9-fold towards PDAC compared to a fast-growing non-cancerous cell line even in high glucose concentration which is further increased by 5-fold more under glucose deprivation. This underscores the potential of glycopolymer delivery vehicle-based **DP@2** for targeting cancer cells with elevated glycolysis rates. Overall, this work broadens the application of Ru complexes with stable curcumin derivatives and demonstrates the feasibility of using RAFT-based glycopolymers to deliver complexes like **2**, which can release the *O,O* donor ligand morphocumin within lysosomes in response to specific stimuli, such as hydrogen peroxide, produced in cancer cells.

Supporting Information Summary

Supporting Information is available from the Wiley Online Library or from the author. The authors have cited additional references within the supporting information.[19,45,64,76,78,81–92]

Acknowledgements

The authors sincerely acknowledge SERB (CRG/2021/001118) for funding. The authors are thankful to IISER Kolkata for instrumental and infrastructural facilities. S.R. thanks DST-INSPIRE, S.P. thanks Govt. of India for Prime Minister Research Fellowship (PMRF) and S.M. thanks KVPY for his BS-MS fellowship.

Conflict of Interests

The authors declare no conflict of interest.

Data Availability Statement

The data that support the findings of this study are available from the corresponding author upon reasonable request.

Keywords: Ruthenium polypyridyl · Chemotherapeutics · Target specificity · Glycopolymer · Micelle

[1] S. Rottenberg, C. Disler, P. Perego, *Nat. Rev. Cancer* **2021**, *21*, 37–50.
[2] T. R. Steel, F. Walsh, A. Wieczorek-Błauż, M. Hanif, C. G. Hartinger, *Coord. Chem. Rev.* **2021**, *439*, 213890.
[3] Pragti, B. K. Kundu, S. Mukhopadhyay, *Coord. Chem. Rev.* **2021**, *448*, 214169.
[4] F. E. Poynton, S. A. Bright, S. Blasco, D. C. Williams, J. M. Kelly, T. Gunnlaugsson, *Chem. Soc. Rev.* **2017**, *46*, 7706–7756.
[5] M. Martínez-Alonso, G. Gasser, *Coord. Chem. Rev.* **2021**, *434*, 213736.
[6] F. H. Burstall, *J. Chem. Soc. (Resumed)* **1936**, *0*, 173–175, DOI: 10.1039/JR9360000173.
[7] H. Dau, C. Limberg, T. Reier, M. Risch, S. Roggan, P. Strasser, *ChemCatChem* **2010**, *2*, 724–761.
[8] M. Jakubaszek, B. Goud, S. Ferrari, G. Gasser, *Chem. Commun.* **2018**, *54*, 13040–13059.
[9] F. Heinemann, J. Karges, G. Gasser, *Acc. Chem. Res.* **2017**, *50*, 2727–2736.
[10] M. Ankathatti Munegowda, A. Manalac, M. Weersink, S. A. McFarland, L. Lilge, *Coord. Chem. Rev.* **2022**, *470*, 214712.
[11] S. Monro, K. L. Colon, H. Yin, J. Roque Iii, P. Konda, S. Gujar, R. P. Thummel, L. Lilge, C. G. Cameron, S. A. McFarland, *Chem. Rev.* **2018**, *119*, 797–828.
[12] A. C. Hachey, D. Havrylyuk, E. C. Glazer, *Curr. Opin. Chem. Biol.* **2021**, *61*, 191–202.
[13] F. Qu, R. W. Lamb, C. G. Cameron, S. Park, O. Oladipupo, J. L. Gray, Y. Xu, H. D. Cole, M. Bonizzoni, Y. Kim, S. A. McFarland, C. E. Webster, E. T. Papish, *Inorg. Chem.* **2021**, *60*, 2138–2148.
[14] S. Bonnet, *Dalton Trans.* **2018**, *47*, 10330–10343.
[15] A. Li, C. Turro, J. J. Kodanko, *Acc. Chem. Res.* **2018**, *51*, 1415–1421.
[16] Curcumin in food supplements: Acceptable daily intake may be exceeded, G. F. I. f. R. A. (BfR) opinion No. 040/2021, **2021**, 1-11, DOI 10.17590/20211221-123422.
[17] M. Kharat, Z. Du, G. Zhang, D. J. McClements, *J. Agric. Food. Chem.* **2017**, *65*, 1525–1532.
[18] H. Ayub, M. Islam, M. Saeed, H. Ahmad, F. Al-Asmari, M. F. Ramadan, M. Alissa, M. A. Arif, M. U. J. Rana, M. Subtain, *Food Sci. Nutrition* **2024**, *12* (11), 8623–8650
[19] S. Roy, P. Mitra, S. Acharya, S. S. Roy, S. Ghosh, M. Maji, N. Modak, N. Ghosh, M. Acharya, S. Singh, *Inorg. Chem. Front.* **2022**, *9*, 5840–5852.
[20] X. Wang, X. Wang, S. Jin, N. Muhammad, Z. Guo, *Chem. Rev.* **2018**, *119*, 1138–1192.
[21] H. Nakamura, K. Takada, *Cancer Sci* **2021**, *112*, 3945–3952.
[22] T. P. Szatrowski, C. F. Nathan, *Cancer Res.* **1991**, *51*, 794–798.
[23] T. Ali, D. Li, T. N. F. Ponnamperumage, A. K. Peterson, J. Pandey, K. Fatima, J. Brzezinski, J. A. R. Jakusz, H. Gao, G. E. Koelsch, *Cancers (Basel)* **2024**, *16*, 2171.
[24] B. Halliwell, J. M. C. Gutteridge, *Free Radicals in Biology and Medicine*, Oxford University Press, USA **2015**.
[25] B. Yang, Y. Chen, J. Shi, *Chem. Rev.* **2019**, *119*, 4881–4985.
[26] Z. Chu, J. Yang, W. Zheng, J. Sun, W. Wang, H. Qian, *Coord. Chem. Rev.* **2023**, *481*, 215049.
[27] M. T. Manzari, Y. Shamay, H. Kiguchi, N. Rosen, M. Scaltriti, D. A. Heller, *Nat. Rev. Mater.* **2021**, *6*, 351–370.
[28] C. Riccardi, D. Musumeci, M. Trifuoggi, C. Irace, L. Paduano, D. Montesarchio, *Pharmaceuticals (Basel)* **2019**, *12*, 146.
[29] J. Karges, *BME Front.* **2023**, *4*, 0024.
[30] E. Villemin, Y. C. Ong, C. M. Thomas, G. Gasser, *Nat. Rev. Chem.* **2019**, *3*, 261–282.
[31] M. H. Stenzel, *Macromolecules* **2022**, *55*, 4867–4890.
[32] N. Pan, Y. Zhang, M. Huang, Z. Liang, Y. Gong, X. Chen, Y. Li, C. Wu, Z. Huang, J. Sun, *JBIC J. Biol. Inorg. Chem.* **2024**, *29*, 265–278.
[33] B. Zengin Kurt, D. Öztürk Civelek, E. B. Cakmak, Y. Kolcuoğlu, H. Şenol, B. m. N. Sağlık Özkan, A. Dag, K. Benkli, *J. Med. Chem.* **2024**, *67*, 4463–4482.
[34] Y. Lu, D. Zhu, Q. Le, Y. Wang, W. Wang, *Nanoscale* **2022**, *14*, 16339–16375.
[35] A. Sánchez, S. P. Mejía, J. Orozco, *Molecules* **2020**, *25*, 3760.
[36] Y. Li, W. Hong, H. Zhang, T. T. Zhang, Z. Chen, S. Yuan, P. Peng, M. Xiao, L. Xu, *J. Controlled Release* **2020**, *317*, 232–245.
[37] E. Dalle Vedove, G. Costabile, O. M. Merkel, *Adv. Healthcare Mater.* **2018**, *7*, 1701398.
[38] E.-H. Song, M. J. Manganiello, Y.-H. Chow, B. Ghosn, A. J. Convertine, P. S. Stayton, L. M. Schnapp, D. M. Ratner, *Biomaterials* **2012**, *33*, 6889–6897.
[39] R. J. DeBerardinis, N. S. Chandel, *Nat. Metab.* **2020**, *2*, 127–129.
[40] S. A. Torres-Pérez, C. E. Torres-Pérez, M. Pedraza-Escalona, S. M. Pérez-Tapia, E. Ramón-Gallegos, *Front. Oncol.* **2020**, *10*, 605037.
[41] H. Martin, L. R. Lázaro, T. Gunnlaugsson, E. M. Scanlan, *Chem. Soc. Rev.* **2022**, *51*, 9694–9716.
[42] L. Conti, E. Macedi, C. Giorgi, B. Valtancoli, V. Fusi, *Coord. Chem. Rev.* **2022**, *469*, 214656.
[43] R. T. Ryan, D. Havrylyuk, K. C. Stevens, L. H. Moore, S. Parkin, J. S. Blackburn, D. K. Heidary, J. P. Selegue, E. C. Glazer, *Eur. J. Inorg. Chem.* **2021**, *2021*, 3611–3621.
[44] P. Srivastava, M. Shukla, G. Kaul, S. Chopra, A. K. Patra, *Dalton Trans.* **2019**, *48*, 11822–11828.
[45] J. Karges, M. Tharaud, G. Gasser, *J. Med. Chem.* **2021**, *64*, 4612–4622.
[46] L. Wang, G. Li, L. Cao, K. Shao, Y. Li, X. Zhang, J. Zhao, W. Zhao, *ACS Pharmacol. Transl. Sci.* **2022**, *5*, 110–117.
[47] R. Gao, H. Xu, L. Liu, Y. Zhang, T. Yin, H. Zhou, M. Sun, N. Chen, Y. Ren, T. Chen, *Biomed. Opt. Express* **2020**, *11*, 4203–4223.
[48] J. R. Aguilar Cosme, D. C. Gagui, N. H. Green, H. E. Bryant, F. Claeyssens, *ACS Biomater. Sci. Eng.* **2021**, *7*, 5078–5089.
[49] M. M. Kim, A. Darafsheh, *Photochem. Photobiol.* **2020**, *96*, 280–294.
[50] A. Chakraborty, S. Roy, M. P. Chakraborty, S. S. Roy, K. Purkait, T. S. Koley, R. Das, M. Acharya, A. Mukherjee, *Inorg. Chem.* **2021**, *60*, 18379–18394.
[51] S. Acharya, M. Maji, M. P. Chakraborty, I. Bhattacharya, R. Das, A. Gupta, A. Mukherjee, *Inorg. Chem.* **2021**, *60*, 3418–3430.
[52] M. Maji, S. Karmakar, Ruturaj, A. Gupta, A. Mukherjee, *Dalton Trans.* **2020**, *49*, 2547–2558.
[53] Ruturaj, M. Mishra, S. Saha, S. Maji, E. Rodriguez-Boulan, R. Schreiner, A. Gupta, *J. Cell Sci.* **2024**, *137*, jcs261258.
[54] X. Xue, Y. Fu, L. He, L. Salassa, L.-F. He, Y.-Y. Hao, M. J. Koh, C. Soulie, R. J. Needham, A. Habtemariam, *Inorg. Chem.* **2021**, *60*, 17450–17461.
[55] L. Kennedy, J. K. Sandhu, M.-E. Harper, M. Cuperlovic-Culf, *Biomolecules* **2020**, *10*, 1429.
[56] Y. Wu, T. Guo, Y. Qiu, Y. Lin, Y. Yao, W. Lian, L. Lin, J. Song, H. Yang, *Chem. Sci.* **2019**, *10*, 7068–7075.

[57] Z. Liu, B. Zhang, S. Xia, L. Fang, S. Gou, *Eur. J. Med. Chem.* **2021**, *212*, 112997.
[58] J. Kasparkova, A. Hernández-García, H. Kostrhunova, M. Goicuría, V. c. Novohradsky, D. Bautista, L. Markova, M. D. Santana, V. Brabec, J. Ruiz, *J. Med. Chem.* **2023**, *67*, 691–708.
[59] Oecd, *OECD Guidelines for the Testing of Chemicals, Section 1: Physical-Chemical Properties* **2022**, Test No. 117: Partition Coefficient (n-octanol/water), HPLC Method.
[60] C. E. Elgar, N. A. Yusoh, P. R. Tiley, N. Kolozsvari, L. G. Bennett, A. Gamble, E. V. Péan, M. L. Davies, C. J. Staples, H. Ahmad, *J. Am. Chem. Soc.* **2023**, *145*, 1236–1246.
[61] S. Li, G. Xu, Y. Zhu, J. Zhao, S. Gou, *Dalton Trans.* **2020**, *49*, 9454–9463.
[62] M. Sirajuddin, S. Ali, A. Badshah, *J. Photochem. Photobiol., B* **2013**, *124*, 1–19.
[63] M. E. Guicciardi, M. Leist, G. J. Gores, *Oncogene* **2004**, *23*, 2881–2890.
[64] K. M. Knopf, B. L. Murphy, S. N. MacMillan, J. M. Baskin, M. P. Barr, E. Boros, J. J. Wilson, *J. Am. Chem. Soc.* **2017**, *139*, 14302–14314.
[65] N. Jariyamana, P. Chuveera, A. Dewi, W. Leelapornpisid, J. Ittichaicharoen, S. Chattipakorn, T. Srisuwan, *Clin. Oral Investigations* **2021**, *25*, 3919–3928.
[66] L. Fetzer, B. Boff, M. Ali, M. Xiangjun, J.-P. Collin, C. Sirlin, C. Gaiddon, M. Pfeffer, *Dalton Trans.* **2011**, *40*, 8869–8878.
[67] W. H. Koppenol, R. H. Hider, *Free Radical Biol. Med.* **2019**, *133*, 3–10.
[68] M. Chrzanowska, A. Katafias, R. van Eldik, *Inorg. Chem.* **2020**, *59*, 14944–14953.
[69] J. M. Suski, M. Braun, V. Strmiska, P. Sicinski, *Cancer Cell* **2021**, *39*, 759–778.
[70] C. J. Sherr, J. Bartek, *Ann. Rev. Cancer Biol.* **2017**, *1*, 41–57.
[71] M. Falck Miniotis, A. Mukwaya, A. Gjörloff Wingren, *PloSOne* **2014**, *9*, e106546.
[72] L. Yan, P. Raj, W. Yao, H. Ying, *Cancers (Basel)* **2019**, *11*, 1460.
[73] M. Achalandabaso Boira, M. Di Martino, C. Gordillo, M. Adrados, E. Martín-Pérez, *BMC Cancer* **2020**, *20*, 1–9.
[74] A. H. Davis-Yadley, A. M. Abbott, J. M. Pimiento, D.-T. Chen, M. P. Malafa, *Pancreas (Philadelphia, PA, U. S.)* **2016**, *45*, 974–979.
[75] H. Ying, A. C. Kimmelman, C. A. Lyssiotis, S. Hua, G. C. Chu, E. Fletcher-Sananikone, J. W. Locasale, J. Son, H. Zhang, J. L. Coloff, H. Yan, W. Wang, S. Chen, A. Viale, H. Zheng, J.-h. Paik, C. Lim, A. R. Guimaraes, E. S. Martin, J. Chang, A. F. Hezel, S. R. Perry, J. Hu, B. Gan, Y. Xiao, J. M. Asara, R. Weissleder, Y. A. Wang, L. Chin, L. C. Cantley, R. A. DePinho, *Cell (Cambridge, MA, U. S.)* **2012**, *149*, 656–670.
[76] S. Kumar, B. Maiti, P. De, *Langmuir* **2015**, *31*, 9422–9431.
[77] M. Kumari, M. Billamboz, E. Leonard, C. Len, C. Böttcher, A. K. Prasad, R. Haag, S. K. Sharma, *RSC Adv.* **2015**, *5*, 48301–48310.
[78] Z. Guo, J. Sui, M. Ma, J. Hu, Y. Sun, L. Yang, Y. Fan, X. Zhang, *J. Controlled Release* **2020**, *326*, 350–364.
[79] Y. H. A. Hussein, M. Youssry, *Materials (Basel)* **2018**, *11*, 688.
[80] N. Nishiyama, K. Kataoka, *Polym. Ther. II* **2006**, *193*, 67–101.
[81] P. A. Lay, A. M. Sargeson, H. Taube, M. H. Chou, C. Creutz, *Inorg. Synth.* **1986**, *186*, 291–299.
[82] G. Moad, Y. K. Chong, A. Postma, E. Rizzardo, S. H. Thang, *Polymer* **2005**, *46*, 8458–8468.
[83] K. Mitra, S. Gautam, P. Kondaiah, A. R. Chakravarty, *Angew. Chem. Int. Ed.* **2015**, *54*, 13989–13993.
[84] P. Kumari, S. Ghosh, S. Acharya, P. Mitra, S. Roy, S. Ghosh, M. Maji, S. Singh, A. Mukherjee, *J. Med. Chem.* **2023**, *66* (20), 14061–14079.
[85] Gaussian 16, Revision B.01, M. J. e. Frisch, G. W. Trucks, H. B. Schlegel, G. E. Scuseria, M. Robb, J. R. Cheeseman, G. Scalmani, V. Barone, G. A. Petersson, H. Nakatsuji, Gaussian, Inc. Wallingford, CT **2016**.
[86] G. Jones, P. Willett, R. C. Glen, A. R. Leach, R. Taylor, *J. Mol. Biol.* **1997**, *267*, 727–748.
[87] M. K. Raza, K. Mitra, A. Shettar, U. Basu, P. Kondaiah, A. R. Chakravarty, *Dalton Trans.* **2016**, *45*, 13234–13243.
[88] K. Mitra, S. Gautam, P. Kondaiah, A. R. Chakravarty, *Eur. J. Inorg. Chem.* **2017**, *2017*, 1753–1763.
[89] A. K. Renfrew, N. S. Bryce, T. W. Hambley, *Chem. Sci.* **2013**, *4*, 3731–3739.
[90] A. K. Renfrew, N. S. Bryce, T. Hambley, *Chem.-A Eur. J.* **2015**, *21*, 15224–15234.
[91] A. Garai, I. Pant, S. Banerjee, B. Banik, P. Kondaiah, A. R. Chakravarty, *Inorg. Chem.* **2016**, *55*, 6027–6035.
[92] A. Jana, B. K. Verma, A. Garai, P. Kondaiah, A. R. Chakravarty, *Inorg. Chim. Acta* **2018**, *483*, 571–578.

Manuscript received: October 26, 2024
Accepted manuscript online: November 30, 2024
Version of record online: December 10, 2024